Eur. Phys. J. D **21**, 323–333 (2002)
DOI: 10.1140/epjd/e2002-00211-3

THE EUROPEAN PHYSICAL JOURNAL D

Charged cores in ionized ^{4}He clusters

I: The $He_2^+ \cdots He$ system

E. Scifoni[1,2] and F.A. Gianturco[1,a]

[1] Department of Chemistry and INFM, University of Rome "La Sapienza", Piazzale A. Moro 5, 00185 Rome, Italy
[2] Dipartimento di Chimica e Chimica Industriale, University of Genoa, via Dodecaneso 31, 16146 Genoa, Italy

Received 25 June 2002 / Received in final form 27 August 2002
Published online 22 October 2002 –

Abstract. Experimental and theoretical studies in large ionic helium clusters have suggested the presence of a diatomic (and occasionally triatomic) charged molecular core surrounded by the other atoms which are bound to it by weaker interactions [1–3]. The understanding of the interactions between the system He_2^+ and an additional He atom of the cluster is therefore important in order to start modelling the full cluster interaction potential. In the present work we carry out a new set of calculations on the full potential and on the bound states supported by the He_2^+ isolated ion and further extend them to generate a Rigid Rotor (RR) potential energy surface (PES) for the triatomic system with He_2^+ kept at its equilibrium geometry (2.0 a.u.). The 13 bound states which were found and the overall angular anisotropy that exists for this Potential Energy Surface (PES) are discussed in detail. We additionally show results of calculations on the surface vibrational extension to nine different values of the He_2^+ interatomic distance, thereby generating a fuller, three-dimensional interaction potential. A simpler modelling of the latter *via* "Pseudo Rigid Rotor" calculations for the bound states with a vibrationally excited core is also presented and discussed.

PACS. 36.40.Wa Charged clusters – 31.50.Gh Surface crossings, non-adiabatic couplings – 31.50.Bc Potential energy surfaces for ground electronic states – 31.15.Ar Ab initio calculations

1 Introduction

Several experiments have been carried out in recent times on helium clusters [1–5] since the possibility of producing them by supersonic expansions in molecular beams and the great interest in the superfluidity features of this solvent make them very intriguing systems to study. A large amount of experimental and theoretical work [6–11] has also been done with neutral helium clusters containing other dopant species, neutral and ionic, embedded in them as impurities.

Helium cluster ions are also very interesting because the enhanced strength of the bonds associated with the He^+ ion constitutes a strong perturbation of the original, weakly interacting van der Waals (VdW) system. Even the simplest MO approach, in fact, is able to clearly identify the He_2^+ as having a chemical bond. It is also important to stress that such ionized aggregates have been the subject of experimental investigations [5] which have provided interesting results and have opened up several theoretical problems that still have not been fully answered.

A fundamental goal of such studies is to obtain reliable information about the structural features of the *ionic core* within each cluster, since the charge is usually thought to be localized over a small number of strongly bound atoms with the surrounding neutral atoms connected to this core by induction and dispersion forces. An important experiment [1], among others [12–14], demonstrated a marked predominance of He_2^+ fragments in the mass spectra of very large ionized aggregates collected after break-up: this large abundance (about 40% of the total) turned out to be independent of the initial size of the cluster. Theoretical studies [2] using the DIM approximation have shown the existence of a linear triatomic core He_3^+ for small clusters ($N < 8$), the coexistence of the two arrangements for some intermediate values ($8 \leq N \leq 12$) and the dominant presence of the He_2^+ for larger systems. Other studies, on the other hand [15,16], have shown the low reliability of using DIM models for helium ions, even if they could be trusted for studies on other rare gas clusters like Ar and Ne. The possibility of obtaining a general structure with the He_2^+ molecule constituting the core appears to be suggested by the fairly strong ionic bond of the He_2^+ moiety. It is known, in fact, that the equilibrium distance in it is much smaller than the neutral He–He average distance in the

[a] e-mail: fa.gianturco@caspur.it

cluster (∼6 a.u.) [17], and that the corresponding dissociation energies are also very different: ∼0.5 meV for the neutral dimer, and ∼2 eV for He_2^+ [18].

It is therefore important to study in detail the microscopic interaction between a single atom and the He_2^+ core, in order to understand better the possible elementary dynamics (see also [3,19]) of the core structure formation shown by the larger clusters. From what we have found in our present study we shall argue that it may be reasonable to assume that, because of the stronger interaction that a single neutral atom experiences with the diatomic charged core as compared to the known atom-atom potential, we might be able to model the whole system of a larger cluster $He_2^+(He)_n$ as chiefly made up of core-atom interactions plus the perturbative effects from the neutral He–He interactions, without having to include contributions from higher order many-body effects. However, this specific aspect of a rather complex problem will be analysed in our future work, limiting our present study to the generation and analysis of an accurate potential energy surface (PES) for an ionic dimer core and an extra helium atom.

2 The theoretical methods

In order to have a coherent picture when studying the interaction in the ionic triatomic system (which we shall limit, for the time being, to producing only a diatomic fragment ion plus a neutral atom in its asymptotic breakup) it is necessary to use a *size consistent* [20] *ab initio* method. In fact failure to ensure the size-consistency property in the calculations would imply that

$$E_{He_2^+(r)He}(R \sim \infty) \neq E_{He_2^+(r)} + E_{He} \tag{1}$$

and hence the interaction energy calculated for this asymptotic channel,

$$V_{He_2^+(r)He}(\mathbf{R}) = E_{He_2^+(r)He}(\mathbf{R}) - E_{He_2^+(r)He}(\infty) \tag{2}$$

(where r is the core interatomic distance and $\mathbf{R}$ the vector measuring distance and orientation of the third atom from the center of mass of the core) will be in error. For this reason, initial calculations carried out using the MRDCI expansion turned out not to be sufficiently accurate. Hence, we further used the Coupled Cluster Method which turned out to be a better choice, provided that the CCSD(T) [21] treatment with aug-cc-pVQZ basis set was employed. All calculations made use of the Gaussian 94 [22] package with the expansion over a basis set that included diffuse functions to yield the aug-cc-pVQZ [23] not present within the code for He atoms. Use of Gaussian 98 with this basis set was inefficient and still showed some problems in its new release. Special attention had to be paid here to the choice of the *guess* functions for those points of the ground state curve of the diatomic system (Σ_u^+ symmetry) which come very close to the dissociative state Σ_g^+: in such situations, in fact, the INDO guess functions employed by the program can lead to sizeable errors. Hence, it became necessary to force the calculations to remain on the lower curve by frequently checking the fragments' asymptotic behaviour, as we shall explain in the next section.

In order to satisfy the expected behaviour in the long range region, it was also important to ensure that the helium atom-dipole polarizability was correctly described by the well-known asymptotic potential (LR) form of the atom-ion interaction

$$E(R)_{\mathrm{LR}} = \frac{1}{2}\alpha_{\mathrm{He}} R^{-4} \tag{3}$$

where the experimental value is here given by $a_{\mathrm{exp}} = 1.38$ a.u. [24].

To further generate the bound states of the He_2^+ moiety we used a simple Numerov [25] algorithm, while for the two-dimensional (2D) problem given by the atom-rigid rotor system ($He_2^+ + He$) where the bound state energies are much weaker, we employed a Discrete Variable Representation expansion method (DVR) [26].

The latter approach involves a well known unitary transformation of a Finite Basis Representation (FBR) defined over some quadrature scheme associated with the FBR polynomials. In our case we used the associated Legendre functions for the angular part and the Morse oscillator-like functions for the radial part, so that one can write

$$H_{\mathrm{DVR}} = T^{\dagger} H_{\mathrm{FBR}} T \tag{4}$$

and the points for the quadrature have been chosen to produce the expected diagonal matrix for the potential representation.

In the present case we have performed calculations with 99 Gauss-Laguerre integration points from 3 to 18 Å on the radial grid, while using 24 points on the angular grid. This method is also suitable for the three dimensional (3D) case by further including additional functions for the vibrational part of the diatomic ion. We are currently carrying out a complete three-particle Potential Energy Surface (PES) description that we shall however analyse in later work.

3 Present results

3.1 The He_2^+ structure

Given the apparent simplicity of this system, the experimental data of recent acquisition are still surprisingly few [27–30]. Some experimental constants have been obtained by extrapolation from the $np\pi\ ^3\Pi_g$ Rydberg series of He_2 and are therefore not very reliable. Its microwave spectrum has been recorded [31], but no direct information about its vibrational and rotational states has become available.

In Figures 1 and 2 we contrast the present calculations (filled-in squares), which use the controlled *guess* functions from the asymptotic region (thereby ensuring a perfect agreement with the dissociative channel energy well into the short-range region), with earlier ones performed without the above constraint (open circles). The

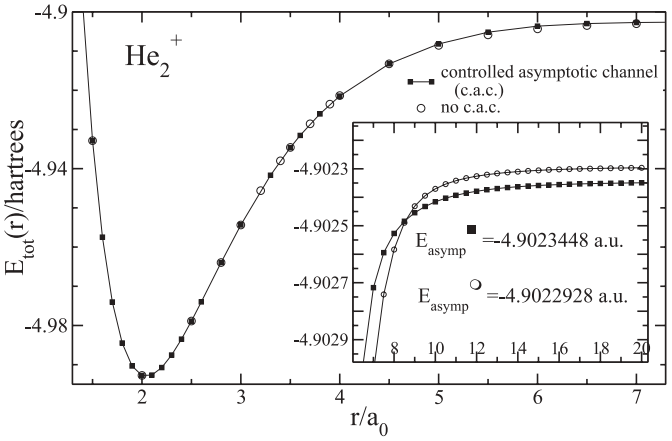

Fig. 1. Computed total energy values for He_2^+ system as a function of its interatomic distance r: previous calculations (open circles) and improved data using a controlled guess function in the evaluation of the two-electron integrals (c.a.c., filled-in squares). In the inset the different asymptotic curves are shown.

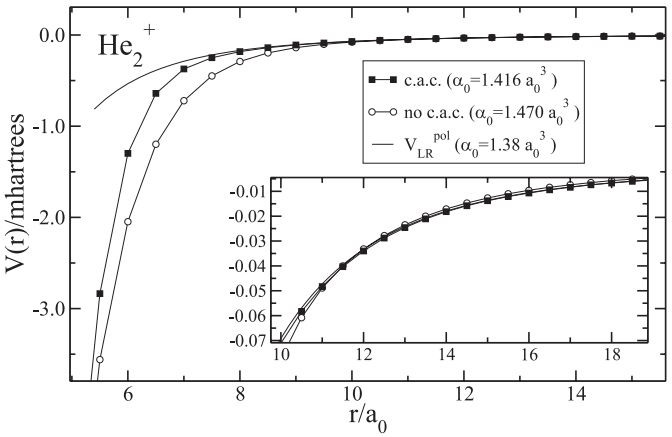

Fig. 2. Interaction energy for the two different approaches of Figure 1 compared in the long range region with the experimental atomic polarizability (α_0) potential. In the legend the extrapolated values for α_0 are also shown.

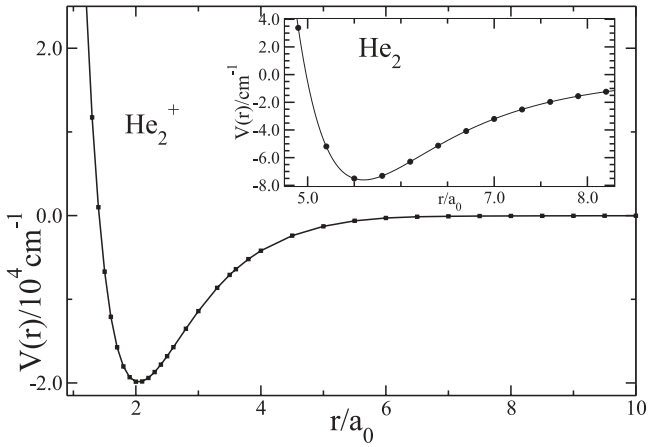

Fig. 3. Computed ground state of the He_2^+ potential energy curve compared (inset) with He_2 potential from reference [32].

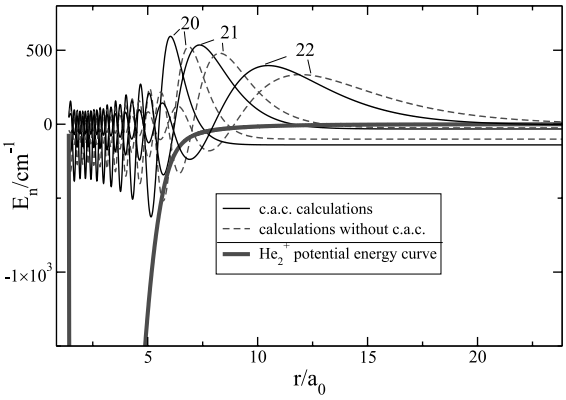

Fig. 4. Computed vibrational wavefunctions of the three upper bound states of He_2^+ (in arbitrary units) superimposed to the top part of the potential well.

size consistency is seen to be verified in the asymptotic region where $E_{He_2^+}(\infty) = -4.9023448$ a.u. $= E_{He^+} + E_{He}$. We also found, with the same method and basis set expansion, that: $E_{He^+} = -1.9998112$ a.u. and $E_{He} = -2.9025336$ a.u., thus giving exactly the same value as that reported before. The open circles produce a slightly different asymptotic value: $E'_{He_2^+}(\infty) = -4.9022928$ a.u.

The extrapolated estimate given for the polarizability by the filled-in squares calculations is also very close to the experiment and yields a better correlation coefficient with the expected R^{-4} analytic potential than the open-circles curve (0.999993 *vs.* 0.9993). This is explicitly shown by Figure 2.

The final Potential Energy Curve (PEC) for the He_2^+ ground state is shown in Figure 3 and compared there with one of the best available He–He curves [32] to show their marked differences. Using Morse interpolation, for instance, we find that the resulting equilibrium distance of the ionic dimer is 2.0432 a.u., in good agreement with the experimental value (2.0416 a.u.) [29] and with other calculations that used the QCISD(T) method (2.0435 a.u.) [33]. We further see clearly that the equilibrium distance of the neutral system is much larger (5.65 a.u.), than that of the ionic dimer, so one could expect that during a sudden ionization process, *e.g.* occurring inside the cluster by electron impact, the distance from the singly ionized He atom to the surrounding neutral atoms is much larger than the equilibrium distance in the ion dimer, a feature which will be further discussed below. The polynomial fit of the dimer ion PEC is available on request from the authors.

In Table 1 we report the 23 bound state energies that we have found by Numerov Integration, as mentioned before, while in Figure 4, we show as an example the wavefunctions of the last three bound states obtained *via* both the calculation approaches discussed in the previous section. For such states we also calculated their average radial size together with its standard deviation and we report them in Figure 5. It is worth mentioning here that the PEC for the neutral dimer shown in Figure 3

Table 1. Computed and "measured" bound states for He_2^+ (all energies in cm^{-1}). ΔE_0 indicates the ZPE value estimated from calculations. The experimental energies are obtained from the experimental D_e, ω_e and $\omega_e x_e$ values by $E_n = D_e + \hbar\omega_e(n + 1/2) - \hbar\omega_e x_e(n + 1/2)^2$.

	c.a.c. results		no c.a.c. results		Experiments [29]	
n	E_n	ΔE_n	E_n	ΔE_n	E_n	ΔE_n
23	-	-	−2.61	19.05	−10.99	74.70
22	−6.20	26.18	−21.66	71.45	−85.69	145.30
21	−32.38	107.47	−93.11	146.43	−230.99	215.90
20	−139.85	239.02	−239.54	226.64	−446.89	286.50
19	−378.88	339.00	−466.18	307.50	−733.39	357.10
18	−717.87	416.86	−773.68	387.93	−1090.49	427.70
17	−1134.73	487.14	−1161.61	467.50	−1518.19	498.30
16	−1621.87	555.77	−1629.11	546.07	−2016.49	568.90
15	−2177.64	625.13	−2175.18	623.55	−2585.39	639.50
14	−2802.77	695.87	−2798.73	700.22	−3224.89	710.10
13	−3498.63	767.46	−3498.95	776.04	−3934.99	780.70
12	−4266.10	839.55	−4274.99	851.09	−4715.69	851.30
11	−5105.65	911.85	−5126.08	925.77	−5566.99	921.90
10	−6017.49	983.49	−6051.85	999.88	−6488.89	992.50
9	−7000.98	1055.94	−7051.73	1072.75	−7481.39	1063.10
8	−8056.92	1128.29	−8124.48	1144.64	−8544.49	1133.70
7	−9185.21	1199.64	−9269.12	1199.26	−9678.19	1204.30
6	−10384.85	1270.17	−10468.38	1306.63	−10882.49	1274.90
5	−11655.02	1340.45	−11775.01	1356.91	−12157.39	1345.50
4	−12995.47	1410.36	−13131.92	1423.63	−13502.89	1416.10
3	−14405.83	1480.24	−14555.55	1494.62	−14918.99	1486.70
2	−15886.06	1550.04	−16050.17	1543.61	−16405.69	1557.30
1	−17436.10	1619.71	−17593.78	1547.44	−17962.99	1627.90
0	−19055.81	836.07	−19141.22	764.44	−19590.89	840.42

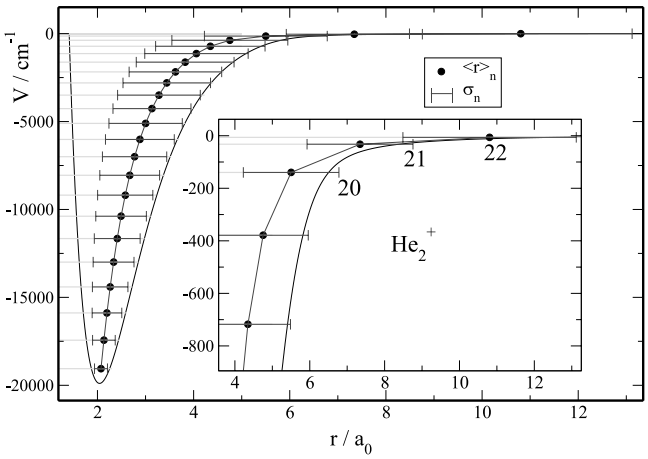

Fig. 5. Radial extension of He_2^+ bound states: for each level (grey lines) the position of the average r value, $\langle r\rangle_n$, and its standard deviation, σ_n, are plotted.

supports instead only one bound state and shows a Zero-Point-Energy (ZPE) value that is about 99% of its well depth [32]. It is also interesting to notice in the data of Figure 5 the high values of the average radial distances exhibited by the last states:

$$\langle r\rangle_{20} = 5.502a_0,$$
$$\langle r\rangle_{21} = 7.342a_0,$$
$$\langle r\rangle_{22} = 10.805a_0.$$

Thus, one may qualitatively expect that a Franck-Condon type of ionization process thought to occur in the neutral helium cluster may lead to dimer-ion-like structures which resemble one of the higher excited levels of the actual dimer ion described by our calculations.

3.2 The He_3^+ rigid rotor system: angular anisotropy and bound states

In order to have a realistic estimate of the most stable structure for the whole triatomic system we performed first a geometry optimization [34] from which we obtain as the global minimum a linear configuration with energy $=-7.902105$ a.u. and distances $R_1 = R_2 = 2.340a_0$. This is very near to the results obtained from previous calculations ($E = -7.902103$, $R = 2.336a_0$) [33].

We then kept the internuclear distance of He_2^+ (r) near its equilibrium value (2.0 a.u., for simplicity) and

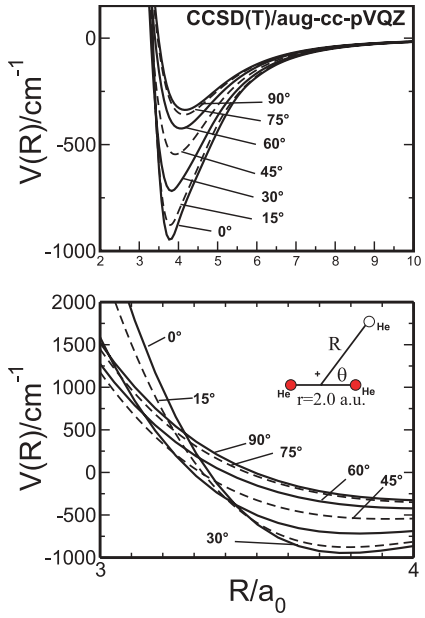

Fig. 6. Calculated angular sections of the $He_2^+(r = 2.0a_0)$−He potential energy surface.

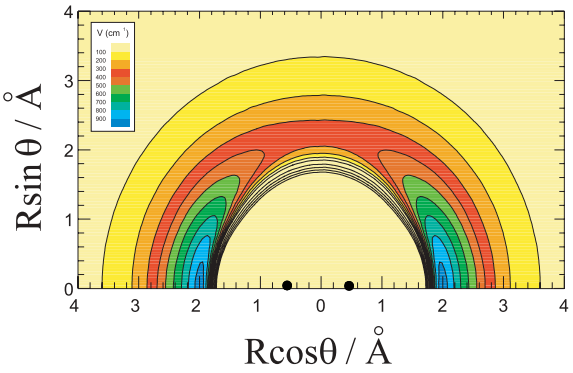

Fig. 7. Interpolated full PES of the $He_2^+(r = 2.0a_0)$−He system in cylindrical coordinates. The two filled-in circles represent the positions of the two helium atoms of the core.

scanned the other Jacobi coordinates (R, the distance from the He_2^+ center of mass to the third He atom, and θ, the angle between R and r). We employed seven angles from 0° to 90° and generated R values from 2.0 to 10.0 a.u., with $\Delta R \leq 0.5a_0$, until we obtained a merging with the analytic long-range potential which uses the experimental polarizability value for all orientations.

The results are pictorially shown in Figures 6 and 7. They exhibit a deep well minimum (-947.16 cm^{-1}) in the linear configuration at $R_{\rm eq} = 3.78$ a.u. By increasing the angle away from the linear geometries we observe a reduction of the minimum depth down to -337.05 cm^{-1}, when we reach a saddle point for $\theta = 90°$ and $R_{\rm min} = 4.17$ a.u. In terms of absolute energy, the linear asymmetric minimum (obtained with the constraint of the $r_{\rm eq}$ fixed distance) lies at -7.8952903 a.u., *i.e.* 548.5 cm^{-1} above the global minimum (linear symmetric) found by optimization calculations (see belove Fig. 10). It therefore seems fairly

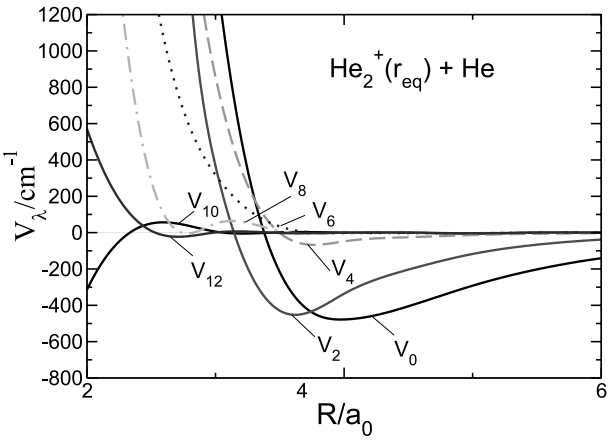

Fig. 8. The seven V_λ curves (from the polynomial expansion: $V_\lambda(R) = 2\pi \int_{-1}^{1} V(R,\theta)P_\lambda(cos\theta)\mathrm{d}\cos\theta)$ for the rigid rotor system.

clear from the above results that the preferred structure for a triatomic cluster will be the linear symmetric one, with the positive charge distributed over the three atoms. For larger clusters containing more ^{4}He atoms the efficiency of the He_2^+ stabilization into its equilibrium structure is likely to become more important because of increased repulsive effects between a larger number of helium atoms. The isoenergetic profiles reported by Figure 7 clearly show the two symmetric minima, the saddle-point region and the highly repulsive core of the triatomic system when He_2^+ is taken to have reached its equilibrium distance.

In Figure 8 we further show the calculated V_λ coefficients of the present PES as obtained from the usual expansion of the Rigid Rotor (RR) potential energy *ab initio* points over Legendre polynomials. One clearly sees the relative greater importance of the lower λ values, with very strong contributions coming from the first anisotropic term, V_2. Using the coefficients obtained up to $\lambda_{\rm max} = 12$, we can then produce a further angular interpolation of the PES as shown by Figure 9. We report in that figure the behaviour of the PES angular derivatives at different R values, where we can see the strong torque acting on the ionic dimer in the small angle regions and at shorter distances. This feature implies strong rotational coupling between the impinging He atom and the ionic dimer in such regions and a weaker coupling along the perpendicular geometry approach. The figure also shows that the interaction essentially becomes angularly isotropic for distances beyond about $6.0a_0$.

Using the DVR method [26] we obtained, for the $J = 0$ angular momentum, the 13 bound states reported in Table 2. The ground state at -596 cm^{-1} lies at about 1/3 of the well depth for the minimum configuration of this triatomic system, and shows, as expected, the strong "chemical" nature of the interaction. We also report in Table 2 the bound states obtained using a completely different integration scheme as described in the BOUND code [35], an outgrowth of the MOLSCAT package, based on molecular scattering equations with different boundary conditions.

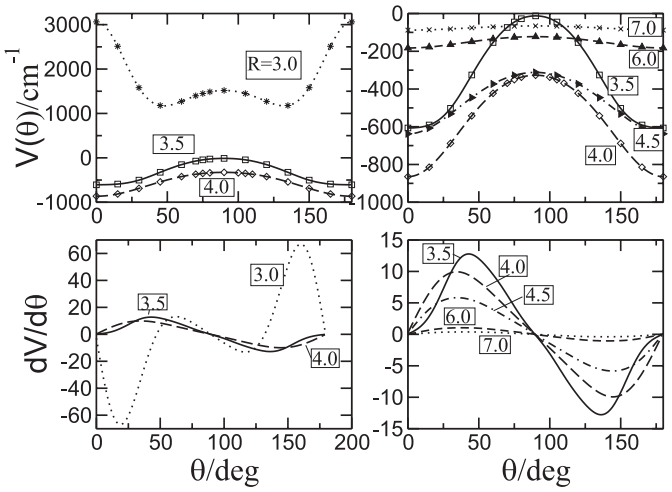

Fig. 9. Angular behaviour of the computed PES and torques generated by the angular coupling, $\partial V/\partial\theta$, for different distances from the center of mass (R) and as a function of the orientation angle θ. The two panels on the right report the values on an enlarged energy scale.

Table 2. Computed bound states for $He_2^+(2.00)-He$ system using the DVR and the BOUND calculations (cm^{-1}). See text for details.

n	E_{DVR}	E_{BOUND}
0	−596.10	−595.50
1	−366.25	−366.94
2	−334.88	−339.49
3	−243.87	−225.69
4	−185.82	−183.03
5	−147.65	−146.23
6	−115.53	−121.05
7	−80.74	−83.44
8	−55.86	−58.13
9	−36.35	−39.16
10	−26.87	−24.71
11	−9.28	−8.17
12	−1.07	−1.19

Previous calculations on the bound states for this system were carried out by a variational analysis of the normal coordinates [33], hence exploring the energy levels in an unconstrained He_3^+ system. In our present study we have taken up, as a zeroth order picture, that of an imperturbed He_2^+ system, thereby keeping its isolated molecular geometry nearly unchanged. A comparison of these earlier results is shown pictorially in Figure 10, where we wish to present a qualitative view of the system and of its different coordinates. The values given in brackets for the set of curves shown in it indicate the internal distances for each system. All the curves are a free-drawn pictorial presentation (not to scale) of the potentials discussed here and are meant to clarify of the present discussion. The energy scale is taken with respect to the minimum energy value of the He_3^+ as given by the optimization calculation (see above). Exper-

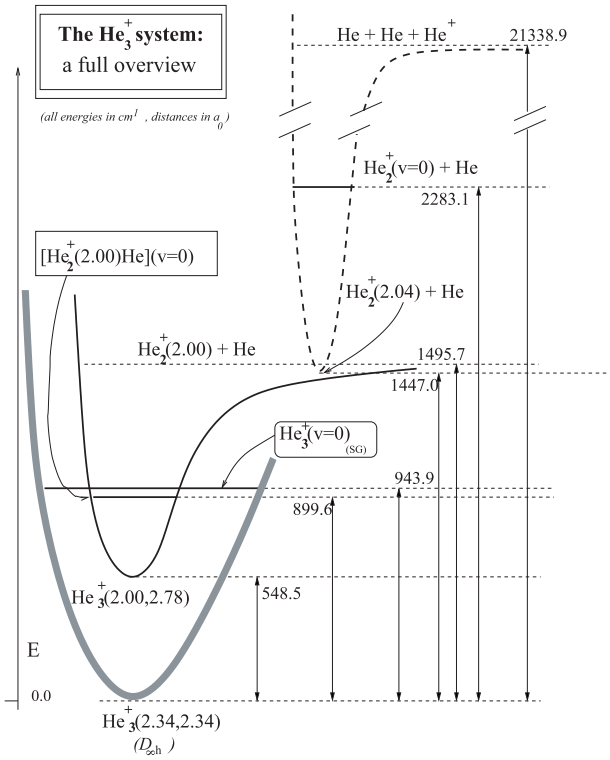

Fig. 10. Schematic representation (not to scale) of the energy profiles of the full He_3^+ system along different possible coordinates: the symmetric normal coordinate of He_3^+ [33] (bold curve), the radial Jacobi coordinate for the rigid rotor surface (solid curve) and the internuclear distance r of He_2^+ (dashed curve). The value labeled "S-G" is from reference [33].

imental data exist for the triatomic system and are due to Patterson [36], while later on Hiraoka and Mori [37] produced the ΔH^0 of the dissociation process: $He_3^+(\nu = 0) \rightarrow He_2^+(\nu = 0) + He$ from thermochemical data on the reaction $He_2^+ + He_2 \rightarrow He_3^+ + He$. Patterson obtained instead [36] the equilibrium constant as a function of temperature and found a value for $D_o = 1371 \pm 161$ cm^{-1}: Hiraoka-Mori reported a value of $D_o = 1305 \pm 52\,cm^{-1}$, having obtained it by pulsed electron-beam mass spectrometer data. These values compare well with our own results: with reference to the computed triatomic ground state energy of reference [33], listed as S–G in Figure 10, we found a value of 1339.2 cm^{-1}, which appears to be within the experimental errors and much better than the values obtained in previous work [38,39]. It is also worth noting that the slight difference found between the value of [33] and our dimer-atom bound state would give a dissociation energy of 1387.9 cm^{-1}, leading to an even better agreement with the Patterson data [36].

We have also computed the spatial shapes of the wavefunctions associated with the bound states of the system. We can see from those reported in Figure 11 that the strong He atom localization shown by the trimer ion ground state in its linear minimum, is gradually reduced through the appearance of inner radial and angular nodes in the upper states, where the associated density now

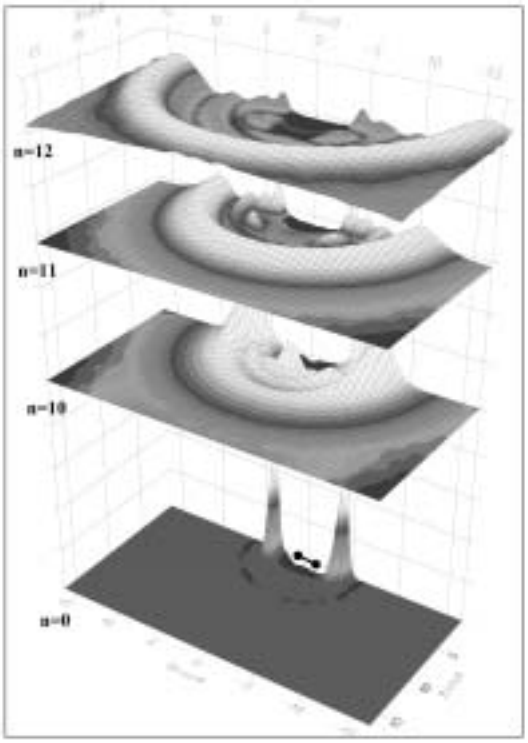

Fig. 11. Computed probability plots for the ground and the three highest bound states of $He_2^+(r = 2.0a_0)-He$ system ($J_{tot} = 0$). The two filled-in circles for the ground state represent the positions of the He atoms in the He_2^+ core (cylindrical coordinates, distances in a_0).

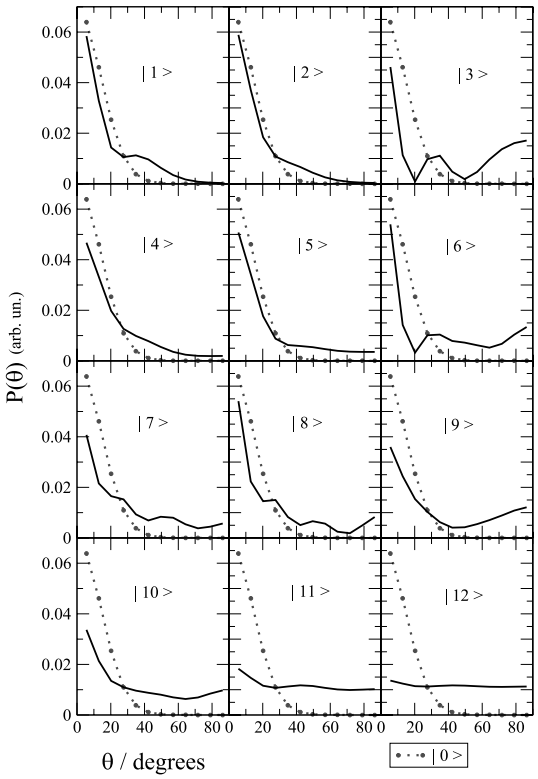

Fig. 12. Angular distributions of the probability densities from the $He_2^+(2.0)-He$ excited bound states obtained from our DVR calculations and compared with that from the ground state (dotted curves).

reveals a strong helium atom delocalization at the outer rims of the molecular space: one sees clearly that the state $n = 12$, for instance, shows a broad, uniform distribution over the whole angular range of the larger radial values. This is particularly clear from the features of the angular atomic densities reported in Figure 12 for all the nuclear bound states, in comparison with those of the ground state, $|0\rangle$, also shown there (dotted curves). One sees that the latter angular density strongly peaks in the small-angle region, to predict the linear minimum configuration, while all the nuclear excited states are increasingly becoming more broadly distributed over the whole angular range, with the higher excited states essentially isotropic over the angular variable. This feature points at a marked delocalization of the additional He atom bound to the He_2^+ core as the system becomes more vibrationally excited. In Figure 13 we further show the radial expectation values for each of the bound states mentioned before. The most striking feature here is again given by the marked size increase shown by the three highest vibrational states. This means that if an additionally bound He atom is placed quite far from the ionic core it will interact with the latter fairly isotropically within a large region of space. The standard deviation values are also shown for each $\langle R\rangle_n$ to further underline the marked increase of delocalization for any additional helium atom when it occupies the upper bound states of the trimer.

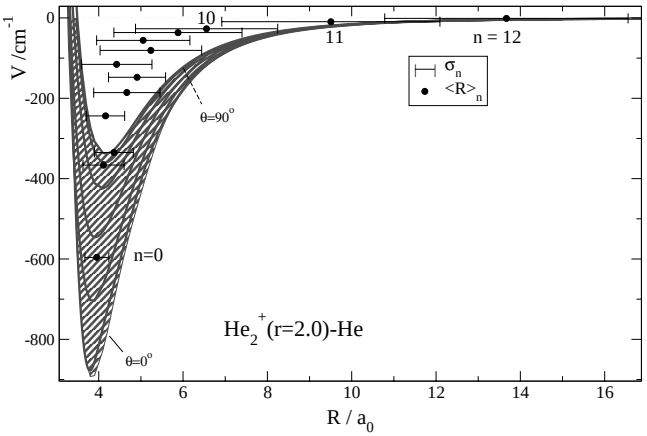

Fig. 13. Radial expectation values for the $[He_2^+(2.0)-He]$ bound states: for each level we plotted the energy position of the $\langle R\rangle_n$, its value and its standard deviation, σ_n. The shaded areas report the PES profiles at different orientation from $\theta = 0^\circ$ and up to $\theta = 90^\circ$.

3.3 The He_3^+ vibrating core system

We further explored additional configurations coming from changes of the ionic dimer bond length by computing 8 different values of the interatomic distance r: from 1.0, to 1.5, 2.5, 3.0, 4.0, 6.0 and $8.0a_0$. The limited importance of the higher V_λ coefficients found from the previous

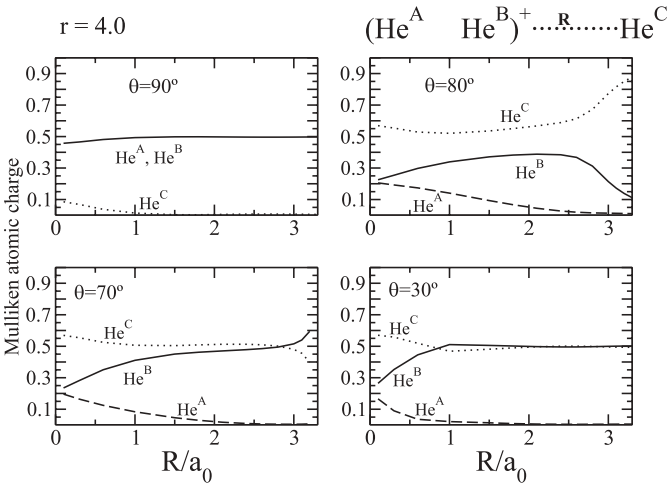

Fig. 14. Mulliken charges from the present calculations for $r = 4.0$ a.u. Four different orientations are shown in the four panels and only the short-range region of the radial variable is reported.

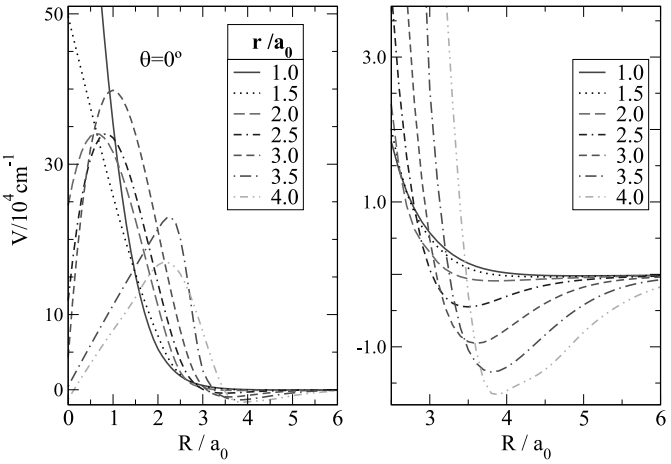

Fig. 15. Potential energy curves for $[He_2^+(r)-He]$ for the $\theta = 0^\circ$ orientation. The different r values are shown in the legend.

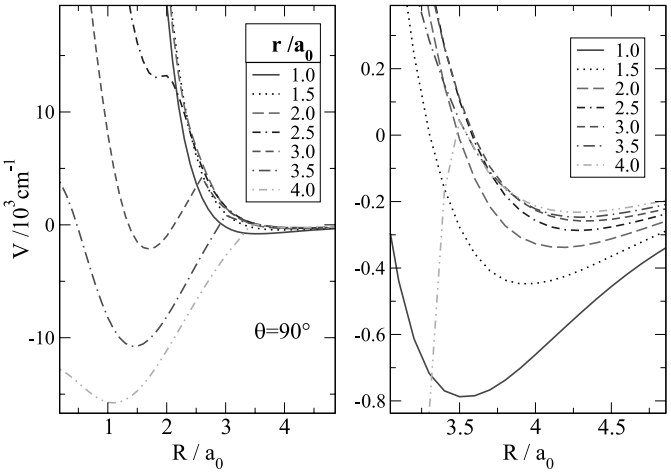

Fig. 16. Same as in Figure 15 but for the $\theta = 90^\circ$ orientation.

expansion led us to surmise that only 4 different angles in the 0–90° range would be sufficient to describe realistically the PES at each fixed value of r. The grid in R was further extended up to 15.0 a.u. in order to produce the correct asymptotic behaviour of the interaction for the larger r values, where the potential well extends over a broader range of R distances. When the internal and intermolecular coordinates become comparable, in fact, it becomes formally meaningless to identify one particular He_2^+ moiety because of the nature of the bonds in this system, which now yield symmetric exchange of the charge within the complex:

$$(He_A He_B)^+ + He_C \longleftrightarrow (He_B He_C)^+ + He_A \longleftrightarrow (He_A He_C)^+ + He_B.$$

This problem affects the calculations for large r values, where we observed some energy discontinuity at short R distances, especially in the perpendicular configurations. In order to understand our results, we therefore examinated the Mulliken charge attributed to each He atom as a function of the R distance for $r = 4.0$ a.u. The results of Figure 14 indicate that along the insertion path for $\theta = 90^\circ$ the charge locates itself symmetrically on the external (A, B) atoms as the third (C) atom enters collinearly in the middle of them (upper-left panel of Fig. 14). For the spatially contiguous C_s structures of approach, also shown in the figure, we see that the calculations instead provide half the charge moving onto the (C) central atom thereby keeping the He_2^+ structure between two contiguous atoms as required here. Hence, by carefully controlling the *guess* functions given for the small-angle approaches, we correctly obtained a consistent energy curve for the 90° approach which was now smoothly going over to the other angles and always produced the correct overall charge distribution for the He_2^+ moiety as described by two directly bound atoms during the dissociation path. The problem is related to a nonadiabatic crossing which is present in the C_{2v} configuration between the nearby $^2A_1$ and $^2B_1$ states, as was extensively discussed in previous work of our group [40] that explored the relevant configurations for this crossing. The feature becomes obviously more evident for larger values of r, because in that case, for $R = 0$, the whole system tends to the global minimum discussed before ($R_1 = R_2 = 2.34a_0$). This electronically nonadiabatic crossing provides an additional fragmentation channel ($He_2 + He^+$) for the system [40,41]: in the ground electronic state the positive charge is distributed over the three centers of the equilibrium geometry, but migrates onto the central atom when moving the relative distances to larger values. In the excited states, however, the charge is carried exclusively by the external atoms along the break-up channel, thereby producing also the He^+ atomic ion.

In Figures 15 and 16 we report two examples of the final results obtained for the full $[He_2^+(r)-He]$ PES for two of the angles and for different r values. It is evident from what we report there that the avoided crossing, present in the C_{2v} configuration, lies in the repulsive region for

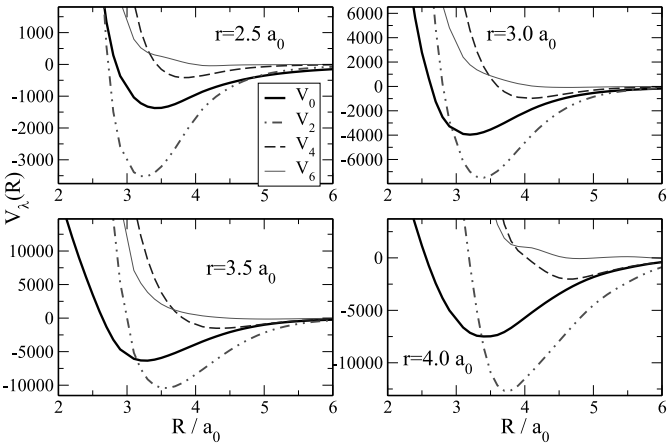

Fig. 17. Computed multipolar coefficients, V_λ, obtained from expansion on the four angles shown in the previous figures. Only four r values are selected in the panels.

small r, while moving out to larger R distances for r values which get to be comparable with R. This particular situation, creates a PES profile, for $r \geq 3.0a_0$, with the appearance of a second minimum at very short range and the progressive reduction of the atom-ion repulsive barrier for larger θ and larger bond distances of the dimer ion.

When looking at the V_λ coefficients for the stretched He_2^+ bond in the complex, given in Figure 17, we see strong contributions from the anisotropic coefficients even for a small stretching of the core geometry. For $r = 2.5a_0$, in fact, the V_2 term is already stronger than the spherical coefficient. Such an effect is probably due to the presence of a "reactive" region in the system which is reached when the three relative distances (r_1, r_2, r_3) become comparable.

One can also profitably consider a sort of "Pseudo Rigid Rotor" system with a "stretched" He_2^+ core kept fixed at an interatomic distance $r_1 > r_{eq}$ during the calculations of the complex bound states. Such a picture implies that a primarily excited ionic dimer core could, to a first approximation, be treated as only weakly distorted by its interaction with the added He atom, especially for the larger R distances. Thus, to compute the PES at $r = 2.5a_0$ means that one is looking at the He_2^+ moiety being already excited around its seventh vibrational level (see Fig. 5) and interacting now with an outer helium atom. The resulting well region turns out to become much deeper than the one associated with the r_{eq} geometry and therefore the number of bound states obtained using the DVR method becomes larger, as reported by Table 3. We further show in Figure 18 the probability density plots of the ground states and of the last three excited states of the "stretched" rotor, together with their radial expectation values. It is interesting to note that the ground state becomes here even more localized and more compact than that in the r_{eq} configuration, signifying a generally attractive effect from the stretching of the ionic core. The higher bound states of the complex, although preserving their delocalized nature over angles as discussed before, are now located closer to its inner core. This strong coupling effect is a signal that at short distances it is not realistic anymore to consider the system as made up from an almost unperturbed diatomic core and an outside, third He atom. It therefore becomes necessary to determine in detail the whole He_3^+ PES using the three strongly correlated Jacobi coordinates which describe it.

Table 3. Computed bound energies, E_n, and energy spacings, ΔE_n, for the [He_2^+(2.50)−He] system. All values in cm^{-1}.

n	E_n	ΔE_n
0	−4044.27	445.22(ZPE)
1	−3333.76	710.51
2	−3244.72	89.04
3	−2657.05	587.68
4	−2572.68	84.37
5	−2478.51	94.18
6	−2017.80	460.71
7	−1940.13	77.66
8	−1855.15	84.99
9	−1777.40	77.75
10	−1420.69	356.71
11	−1354.46	66.22
12	−1283.18	71.28
13	−1220.05	63.13
14	−1168.70	51.35
15	−892.32	276.38
16	−828.77	63.56
17	−781.73	47.04
18	−739.95	41.78
19	−685.00	54.95
20	−607.24	77.75
21	−496.05	111.20
22	−440.04	56.01
23	−389.18	50.86
24	−322.13	67.06
25	−252.35	69.78
26	−243.06	9.29
27	−204.96	38.09
28	−178.00	26.96
29	−151.42	26.57
30	−116.54	34.88
31	−84.84	31.70
32	−82.81	2.03
33	−70.63	12.18
34	−42.72	27.91
35	−32.26	10.46
36	−13.15	19.11
37	−2.49	10.65

4 Present conclusions

We have computed and analyzed in detail a new, accurate potential energy profile of the He_3^+ system and found it to be in good agreement with available experimental data [36,37] and with earlier, more limited calculations.

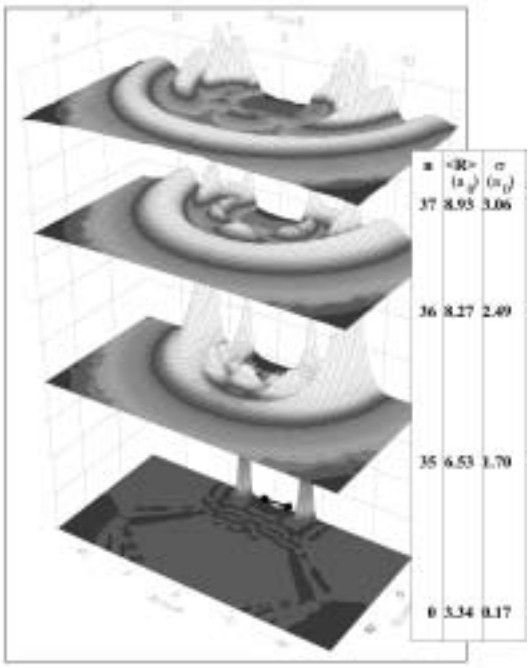

Fig. 18. Probability densities and radial observables for the ground and the three highest bound states (DVR) for the $[He_2^+(r = 2.5a_0)-He]$ system, $J_{tot} = 0$. The two filled-in circles on the ground state represent the positions of the two He atoms in the He_2^+ stretched core (distances in a_0).

We have seen from our analysis that quite a bit of information could already be obtained from the a fixed-nuclei dimer ion calculations, the most important of them being the confirmation of the expected isotropic long-range interaction of such ionic core with an additional He atom when the system is vibrationally hot: such a picture could be already used to understand, at the qualitative level, the experimental evidence found for the existence of such a core in larger ionic clusters: the many additional adatoms could all equally contribute to collisionally "cooling off" the excited dimer moiety produced by single-atom ionization in the neutral clusters. Our recent model calculations for the time-dependent evolution of the trimer photoionization [42] indeed point to the production of highly excited He_2^+ ions after the primary process.

Extending our calculations to a vibrating core reveals the nonadiabatic crossing between $^2A_1$ and $^2B_1$ states which is present in the C_{2v} configuration. For a "stretched core" system, within an adiabatic picture of the interaction between a vibrationally excited He_2^+ and another He atom, we also found a broad angular delocalization for the "hot" vibrational states that indicates again the possible formation of a transient bound state with the surrounding atoms located isotropically within the larger clusters considered in the experiments [1].

All the above is, of course, still rather speculative and we further need to employ the present PES to provide detailed dynamical data at a more quantitative level. They could be obtained for the microscopic process of ionic nucleation by employing the present PES for a quantum study of the collisional inelastic dynamics within the cluster. This is currently in progress and will be reported by our group in a following publication focussed on the collisional cooling dynamics after initial ionization [43].

The actual polynomial interpolation coefficients for the multipolar expansion representing the Rigid-Rotor PES are available on request from the authors.

The financial supports of the University of Rome Research Committee, of the Ministry for University and Research (MUIR) Collaborative Grants Committee and the Max-Planck Gesellschaft are gratefully acknowledged. We are also grateful to one of the referees who has kindly revised the original manuscript and generously help to clarify our presentation.

References

1. B. Callicoatt *et al.*, J. Chem. Phys. **109**, 10195 (1998)
2. P. Knowles, J. Murrel, Mol. Phys. **87**, 827 (1996)
3. M. Ovchinnikov, B.L. Grigorenko, K.C. Janda, V.A. Apkarian, J. Chem. Phys. **108**, 22 (1998)
4. *Clusters of Atoms and Molecules*, edited by H. Haberland (Springer-Verlag, Berlin Heidelberg, 1994)
5. *Cluster ions*, edited by C.Y. Ng, T. Baer, I. Powis (John Wiley & Sons, New York, 1993)
6. K.K. Lehmann, Mol. Phys. **97**, 645 (1999)
7. F. Paesani, K.B. Whaley, F.A. Gianturco, J. Chem. Phys. **115**, 10225 (2001)
8. B. Balta, F.A. Gianturco, F. Paesani, Chem. Phys. **254**, 215 (2000)
9. F. Filippone, F.A. Gianturco, Europhys. Lett. **44**, 585 (1998)
10. V. Ariyente, I. Baccarelli, B. Balta, F.A. Gianturco, C. Selçuki, *Quantum Systems in Physics and Chemistry*, edited by R. Mc Weeny, R. Wilson (Kluwer Academic Publ., Dordrech, 1998)
11. J.P. Toennies, A.F. Vilesov, Annu. Rev. Phys. Chem. **49**, 1 (1998)
12. H. Buchenau, E.L. Knuth, J.A. Northby, J.P. Toennies, C. Winkler, J. Chem. Phys. **92**, 6875 (1990)
13. H. Buchenau, J.A. Northby, J.P. Toennies, J. Chem. Phys. **95**, 8134 (1991)
14. J. Gspann, H. Vollmar, J. Low Temp. Phys. **45**, 343 (1981)
15. F.X. Gadea, I. Paidarova, Chem. Phys. **209**, 281 (1996)
16. F.Y. Naumkin, P.J. Knowles, J.N. Murrell, Chem. Phys. **193**, 27 (1995)
17. M.V. Rama Krishna, K.B. Whaley, J. Chem. Phys. **93**, 6738 (1990)
18. M.V. Rama Krishna, K.B. Whaley, J. Chem. Phys. **93**, 746 (1990)
19. N. Halberstadt, K.C. Janda, Chem. Phys. Lett. **282**, 409 (1998)
20. J.A. Pople, J.S. Binkley, R. Seeger, Int. J. Quant. Chem. Symp. **10**, 1 (1976)
21. J.A. Pople, M. Head-Gordon, K. Ragavachari, J. Chem. Phys. **87**, 5968 (1987)
22. *Gaussian 94*, Revision D.1, M.J. Frisch, G.W. Trucks, H.B. Schlegel, P.M.W. Fill, B.G. Johnson, M.A. Robb, J.R. Cheeseman, T.A. Keith, G.A. Petersson, J.A.

Montgomery, K. Raghavachari, M.A. Al-Laham, V.G. Zakrzewski, J.V. Ortiz, J.B. Foresman, J. Cioslowski, B.B. Stefanov, A. Nanayakkara, M. Challacombe, C.Y. Peng, P.Y. Ayala, W. Chen, M.W. Wong, J.L. Anders, E.S. Replogle, R. Gomperts, R.L. Martin, D.J. Fox, J.S. Binkley, D.J. Defrees, J. Baker, J.P. Stewart, M. Head-Gordon, C. Gonzalez, J.A. Pople, Gaussian Inc., Pittsburgh PA, 1995
23. T.H. Dunning Jr, J. Chem. Phys. **90**, 1007 (1989)
24. U. Hohm, Mol. Phys. UK **69**, 803 (1990)
25. J.W. Cooley, Math. Comp. **5**, 363 (1961)
26. J. Tennyson *et al.*, Comp. Phys. Comm. **86**, 175 (1995)
27. M.L. Ginter, D.S. Ginter, J. Chem. Phys. **48**, 2284 (1968)
28. M.L. Ginter, R. Battino, J. Chem. Phys. **52**, 4469 (1970)
29. M.L. Ginter, C.M. Brown, J. Chem. Phys. **56**, 672 (1972)
30. P.M. Dehmer, S.T. Pratt, J. Chem. Phys. **77**, 4804 (1982)
31. A. Carrington, C.H. Pyne, P.J. Knowles, J. Chem. Phys. **102**, 5979 (1995)
32. R.A. Aziz, F.R.W. McCourt, C.C. Kwong, Mol. Phys. **61**, 1487 (1987)
33. M.F. Satterwhite, G.I. Gellene, J. Chem. Phys. **99**, 13397 (1995)
34. C. Peng, P.Y. Ayala, H.B. Schlegel, M.J. Frisch, J. Comp. Chem. **17**, 49 (1996)
35. J.M. Hutson, *BOUND computer code*, Version 5, October 93, CCP6, SERC Science & Engeneering Research Council (UK)
36. P.L. Patterson, J. Chem. Phys. **48**, 3625 (1968)
37. K. Hiraoka, T. Mori, J. Chem. Phys. **92**, 4408 (1990)
38. V. Staemmler, Z. Phys. D: At. Mol. Clust. **16**, 219 (1990)
39. M. Rosi, C.W. Bauschlicher, Chem. Phys. Lett. **159**, 479 (1989)
40. F.A. Gianturco, M.P. de Lara-Castells, F. Schneider, J. Chem. Phys. **107**, 1522 (1997)
41. F.A. Gianturco *et al.*, Chem. Phys. Lett. **259**, 641 (1996)
42. M. Satta, E. Scifoni, F.A. Gianturco, submitted to J. Chem. Phys.
43. E. Scifoni, E. Bodo, F.A. Gianturco, in preparation